Surface Free Energy of Cubic Boron Nitride Films Deposited on Nanodiamond

ARTICLE *in* THE JOURNAL OF PHYSICAL CHEMISTRY C · AUGUST 2007

Impact Factor: 4.77 · DOI: 10.1021/jp0732561

Surface Free Energy of Cubic Boron Nitride Films Deposited on Nanodiamond

A. Spiesser,[†,‡] Y. M. Chong,[§] K. M. Leung,[†,§] G. Abel,[||] G. G. Ross,[||] M. J. Walzak,[†] R. Jacklin,[†] W. M. Lau,[†] W. J. Zhang,[§] and I. Bello*[,†,§]

Surface Science Western (SSW), University of Western Ontario, London, Ontario, Canada, INRS Energie, Materiaux et Telecommunications, Quebec, Canada, and Center Of Super-Diamond and Advanced Films (COSDAF) & Department of Physics and Materials Science, City University of Hong Kong, Hong Kong SAR, China

Received: April 27, 2007; In Final Form: June 8, 2007

Thin and thick cubic boron nitride (cBN) films were grown on nanodiamond (nanoD), using radio-frequency magnetron sputtering and plasma-enhanced chemical vapor deposition. The chemical composition of the cBN surface layer was nearly stoichiometric, which yielded an essentially pure cubic phase. The root-mean-square roughness of the nanoD and cBN films varied from 4 to 37.5 nm, depending on the pretreatment, method of deposition, and film thickness. The surface free energy of the cBN films with respect to the nanoD was determined by the contact angle measurements. The surface free energy was affected by surface roughness, but the surface energy of nanodiamond was always slightly higher than that of cBN films. This relationship between the surface free energies has important implications for material compatibility and possible local heteroepitaxial growth of cBN on nanoD.

Introduction

Cubic boron nitride (cBN) has drawn considerable attention because its physical and chemical properties are extreme and very comparable to those of diamond.[1,2] Cubic BN has a high atomic density, an extreme hardness, a high chemical stability,[3] a wide band gap,[4] and a high thermal conductivity.[5] These properties, together with presumed high electron and hole mobility, and particularly the ability to dope the films for n- or p-type conductivity, makes cBN an extremely important material for many mechanical, tribological, electronic, optoelectronic, and optical applications. Nevertheless, practical applications of cBN films have been hampered by their poor quality, low phase purity, high compressive stress, poor adhesion, small deposited area, and limited film thickness ($\leq$200 nm).[6−9] These obstacles are induced by the extreme physical properties of cBN, which requires an energetic particle bombardment to form the cubic phase, as well as the need to grow cBN via amorphous and turbostratic BN (aBN/tBN) interfacial layers on most substrates. However, recent experiments demonstrate that adherent cBN films can be grown directly on diamond in local epitaxial relationships, i.e., without aBN/tBN interfacial layers.[10,11] Particularly, electron cyclotron resonance plasma-enhanced chemical vapor deposition (ECR PECVD) employing fluorine chemistry[12−15] has led to impressive results. Because the properties of cBN are closest to those of diamond, it is not surprising that diamond can serve as a most suitable substrate. On the basis of their similar characteristics, one could presume epitaxial growth. However, cBN in the form of films is nanocrystalline, and it is structurally similar to nanodiamond (nanoD). Therefore, this study focuses on the determination of the relative surface energies of cBN and nanoD to explore the viability of growing cBN on nanoD in a local epitaxial relationship.

Experimental Methods

Two sets of 3 μm thick nanoD films were prepared on silicon substrates by microwave plasma CVD in a methane/hydrogen gas mixture with molecular ratio $H_2/CH_4 = 1/9$ using a microwave power of 1.2 kW and a temperature of 800 °C. During growth, a pressure of 30 Torr was maintained. Prior to deposition, the silicon substrates were pretreated by either ultrasonic agitation in the presence of diamond powder (sample E) or mechanical polishing using diamond powder (sample D).

Sample D was used as the substrate to grow a 2.5 μm thick cBN film by ECR PECVD, resulting in sample A. Sample E, with the smoother morphology, was used as the substrate to grow a 500 nm thick cBN film by ECR PECVD, resulting in sample B. A 500 nm thick cBN film was also grown by sputter deposition on sample E, resulting in sample C. A summary of the sample descriptions is presented in Table 1.

ECR PECVD was employed using a gas mixture of helium, argon, nitrogen, boron trifluoride, and hydrogen in the following ratio: $He/Ar/N_2/BF_3/H_2 = 140/10/50/1.5/3$. The plasma was generated using a 1.5 kW ASTeX microwave source. The sample effective bias voltages were −22 and −32 V (external bias voltages −20 and −30 V, plasma potential 2 V). The substrate temperature and operational pressure were maintained at approximately 1000 °C and 2×10^{-3} Torr, respectively. At effective bias voltages of −22 and −32 V the deposition rates were 300 and 350 nm/h, respectively.

Sample C was deposited on the 3 μm thick nanoD (sample E) by radio-frequency magnetron sputtering (RF-MS) at a target-to-substrate distance of 4.5 cm. An rf power of 250 W was applied to a high-purity pyrolytic hBN target. Sputtering was carried out in a gas mixture of argon and nitrogen with a molecular ratio of 2/1 and at an operational pressure of 16

* To whom correspondence should be addressed. E-mail: apibello@cityu.edu.hk.
[†] University of Western Ontario.
[‡] On leave from Ecole Supérieure d'Ingénieurs de Luminy, Marseille, France.
[§] City University of Hong Kong.
[||] INRS Energie, Materiaux et Telecommmunications.

10.1021/jp0732561 CCC: $37.00
Published on Web 08/03/2007

TABLE 1: Sample Descriptions

sample A	sample B	sample C	sample D	sample E
2.5 μm cBN deposited on sample D by ECR	500 nm cBN deposited on sample E by ECR	500 nm cBN deposited on sample E by sputtering	3 μm nanoD deposited on mechanically polished Si	3 μm nanoD deposited on ultrasonically agitated Si

TABLE 2: Rms Surface Roughness Measured for Different cBN and NanoD Films

	sample A, 2.5 μm cBN, CVD	sample B, 500 nm cBN, CVD	sample C, 500 nm cBN, sputtered	sample D, 3 μm nanoD, polished	sample E, 3 μm nanoD, ultras agit
rms roughness (nm)	37 ± 2.5	10 ± 2	6 ± 1	5 ± 1	4 ± 1

mTorr. The substrate was independently biased using a 333 kHz generator that induced a dc voltage offset of -35 V, while the plasma potential was measured to be 15 V. During deposition the substrate was heated to 1000 °C using a 2.0 kW boralectric heater. The deposition rate of cBN was 80 nm/h.

Prior to determination of the surface energies, some structural and chemical properties of both the cBN and nanoD films were examined. The structure of the cBN films was investigated by Fourier transform infrared (FTIR) spectroscopy in transmittance mode using a Bruker IFS55 spectrometer. Background spectra were collected using a bare silicon wafer as the reference. All spectra presented in this work were obtained with nonpolarized light at a normal incidence angle. The FTIR spectra were measured with a 4 cm^{-1} spectral resolution within a wavelength range of 600$-$2000 cm^{-1}.

Raman spectral analyses were performed with a Renishaw UV Raman microscope equipped with a UV Fred 90 laser. For these experiments, the UV laser was operated at 244 nm with a spectral resolution of 1 cm^{-1} and spatial resolution of approximately 1 μm. The laser power was 35 mW and the spot size approximately 5 μm. All Raman measurements were carried out at room temperature. For each spectrum, 10 scans (accumulation time 10×60 s) were collected with the cosmic ray removal program in place.

The elemental composition of the BN samples was determined by X-ray photoelectron spectroscopy (XPS) using a monochromatic Al Kα X-ray source operating at 1486.6 eV. Neither sputter-cleaning nor sputter-profiling was performed in order to retain the intrinsic topographic structure and property being in fact used for contact angle measurements.

The surface topography and roughness, evaluated as a root-mean-square (rms) surface roughness, were studied using a PSIA XE-100 atomic force microscope. The measurements were carried out in noncontact mode at a scan rate of 1 Hz. The field of view was 5×5 μm with 256×256 pixels.

The surface free energies of both nanoD and cBN films were determined by the measurement of the contact angle. The advancing and receding contact angles were measured by increasing and then decreasing the volume of a drop of liquid deposited on the sample surface through a calibrated microsyringe and a programmable pump system. The polar and dispersive contributions to the surface energy were obtained by means of four test liquids (water, diiodomethane, ethylene glycol, and glycerin). Recorded images were digitized and analyzed by means of an Acquidam software that evaluates the tangent at the point of contact between the drop and the surface (i.e., the contact angle). Typically, the maximum volume of the drop is 10 μL. The precision of the contact angle measurement is $\pm 1°$.

Results and Discussion

FTIR spectra (Figure 1) collected from samples A, B, and C are characteristic of cBN, with intense and broad absorption peaks, centered at wavelengths of approximately 1095, 1085, and 1086 cm^{-1}, respectively. These peaks are representative of a cBN structure grown on nanoD films. Broadening of the peaks and flat minima are common in thick cBN films[16] as there is progressively less transmittance of the IR radiation through the sample with increasing film thickness. The reststrahlen (residual radiation) band at the higher wavenumber side is formed due to the interaction of the infrared signal with the optical phonon, which results in a strong absorption. The IR light between the LO and TO modes of cBN is therefore nontransmissible through the cBN lattice when the film is very thick. Estimation of the quality of cBN films, based on the full width at a half-maximum of the absorption peak, is unreliable because one is unable to determine the true line shape in light of the lack of transmittance of the IR radiation through the thicker cBN films. A smaller peak forming a shoulder on the cBN peak, seen in the spectrum of sample A, originates in the hBN phase.[17]

The Raman spectra, presented in Figure 2, were collected from both the 2.5 μm thick and 500 nm thick cBN films. The spectrum of sample A reveals two peaks located at 1056 and 1308 cm^{-1} which denote scattering by the TO and LO phonon modes of cBN,[18] whereas the hBN phonon mode expected at $\sim$1380 cm^{-1} can hardly be observed. The spectrum of sample B shows an intense peak centered at $\sim$1331 cm^{-1} that designates diamond. The peak centered at $\sim$1377 cm^{-1} arises from the hBN E_{2g} mode, although hBN is undetectable in the corresponding FTIR spectrum as the UV Raman spectrum is far more sensitive to the hBN phase than the cBN phase.[18] The Raman signal located at $\sim$1077 cm^{-1} is assigned to the TO phonon mode of cBN. The cBN LO mode cannot be resolved because of its interference with the far more intense diamond peak. The shift in the peak position of the cBN TO mode is caused mainly by the small size of crystallites and/or defects present in the films.[19] The Raman signature thus represents a thick, high-quality cBN film synthesized on nanoD by ECR PECVD at a bias of -32 V, which correlates well with the FTIR analysis. In addition, the UV Raman spectra also show that the film below the cBN is indeed nanodiamond.

The XPS elemental analysis reveals that the B/N ratio is practically equal to unity, which is a fundamental prerequisite for the growth of cBN films. The major contaminants are surface-adsorbed oxygen (5%) and hydrocarbons (18%) coming from the exposure of the samples to the ambient atmosphere.

Since surface roughness can affect the measurement of contact angles and, consequently, the measured surface free energies, surfaces with different roughnesses were produced by employing different substrate pretreatments, i.e., mechanical polishing and ultrasonic agitation with diamond powders. Dissimilarity between the PVD sputter method using a higher effective bias and the PECVD method, employing low bias voltages, gives rise to differences in the surface roughness. To have cBN films with different roughness levels, thin and thick cBN films were

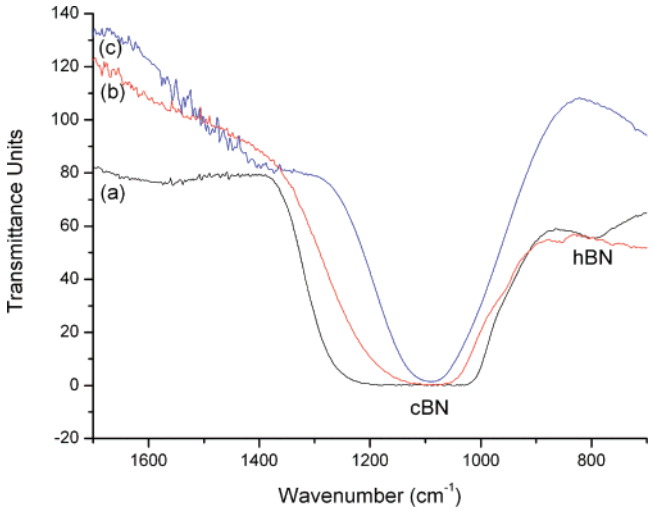

Figure 1. FTIR spectra of (a) a 2.5 μm thick cBN film (sample A) grown on sample D (3 μm nanoD pretreated by mechanical polishing) and (b) a 500 nm thick cBN film (sample B) grown on sample E (3 μm nanoD pretreated by ultrasonic agitation) by ECR PECVD at external bias voltages of −30 V (effective bias −32 V) and −20 V (effective bias −22 V), respectively, and (c) FTIR spectrum of a 500 nm thick cBN film (sample C) prepared on sample E by magnetron sputtering at an external bias voltage of −35 V (−50 V effective bias).

TABLE 3: Dispersion and Polar Components and Surface Free Energy of Different Liquids Used in Contact Angle Measurement (mJ/m²)

liquid	dispersion component	polar component	surface free energy	surface free energy, measured
water	21.8	51	72.8	70.3
glycerol	34	30	64	62
ethylene glycol	29	19	48	46.1
diiodomethane	46.6	4.2	50.8	48

also prepared. The rms surface roughness data for the cBN and nanoD films used in this study, as determined by AFM, are presented in Table 2. The data are also presented in Figure 3 for correlation with the surface free energies. Although the nanodiamond in sample E was grown using deposition parameters identical to those of sample D, sample E exhibits a smoother surface morphology. The pretreatment of the silicon substrate by ultrasonic agitation with diamond powder yields a smoother surface. Cubic BN films (sample C) prepared by RF magnetron sputtering at an effective bias voltage of −50 V (external bias −35 V and plasma potential 15 V) gives the smoothest cBN film morphology likely because of the high kinetic energy of the impinging ions used in the growth process. The films grown by ECR PECVD result in characteristic, larger crystallites, which, in turn, give a rougher surface morphology. The size of the crystallites and, thus, the surface roughness increase with increasing film thickness as is seen in the comparison between samples A and B. Hence, differences in the surface roughness can cause discrepancies in the measured surface free energies.

A dynamic method was used to measure the contact angle of liquids with nanoD and cBN surfaces. The average values of the advancing contact angles were calculated using the Acquidam computer program. The surfaces of all the cBN samples were hydrophilic in nature as seen by the contact angles using distilled water as the probe liquid. The contact angles range from 66° to 78°. The rougher film surfaces exhibit larger contact angles.

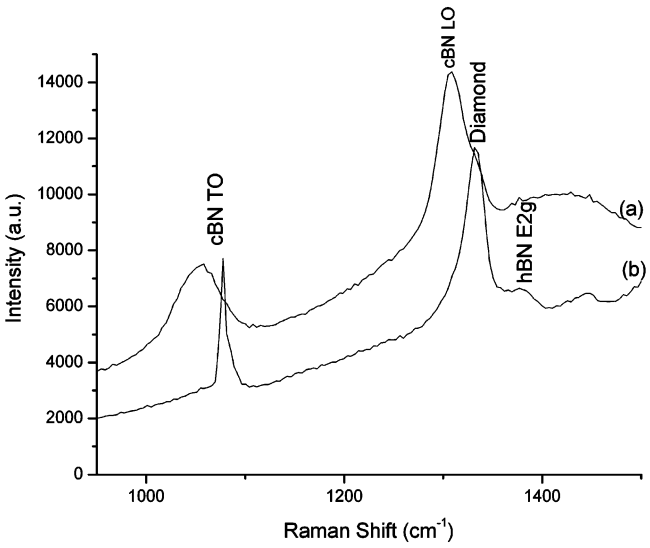

Figure 2. UV Raman spectra collected from (a) sample A, a 2.5 μm thick cBN film deposited at a −32 V effective bias, and (b) sample B, a 500 nm thick cBN film grown at a −22 V effective bias.

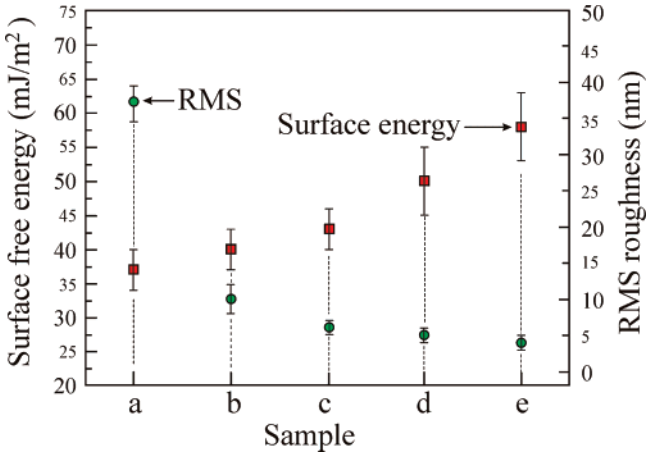

Figure 3. Relative surface free energies and rms surface roughness of cBN and nanoD films: a, (sample A) 2.5 μm thick cBN; b, (sample B) 500 nm thick cBN film; c, (sample C) 500 nm cBN film; d, (sample D) 3 μm thick nanoD film; e, (sample E) 3 μm thick nanoD film.

The surface free energies of cBN samples with reference to nanoD were calculated using data obtained from contact angle measurements. In accordance with Young's equation,[20] Fowkes theory,[21] and Owen and Wendt theory,[22] the polar and dispersion contributions to the solid surface energy can be determined using the following equation:

$$\sigma_l(1 + \cos\theta) = 2(\sigma_s^d \sigma_l^d)^{1/2} + 2(\sigma_s^p \sigma_l^p)^{1/2}$$

where θ is the advancing contact angle, σ_l is the surface energy of the liquid, σ_l^d and σ_l^p are the dispersion and polar contributions to the liquid surface energy, and σ_s^d and σ_s^p are the dispersion and polar contributions to the surface energy of the solid. The probe liquids used (water, diiodomethane, ethylene glycol, and glycerin) cover a wide range of properties from very polar water to very dispersive diiodomethane. These properties are summarized in Table 3. These liquids were verified using the "De Nouy ring" method, which employed a platinum−iridium ring immersed into each liquid. Then the interfacial tension was determined by measuring the required force to break the contact between the ring and liquid. The mean σ_s^d and σ_s^p were determined from the calculated values, and the composite

surface free energy σ_s was calculated from the sum of these mean values. Figure 3 shows the surface free energies of all the samples.

Three independent measurements were averaged to obtain a mean value of the contact angle. Pair values of the angles, in all solid−liquid combinations, were used for setting two equations to calculate the dispersion and polar contributions to the surface energies as shown in Table 3. It should be noted that calculated free energies are not absolute. However, they are good enough to evaluate the possibility of local heteroepitaxial growth since the surface free energy was determined for both cBN and nanoD samples in the same experimental set. The measured contact angles have a 3−4% uncertainty that primarily arises from surface nonuniformity with respect to the chemical composition, surface roughness, and surface flatness of the substrates.

Local epitaxial growth of cBN on polycrystalline diamond has been demonstrated previously using high-resolution transmission electron microscopy (HRTEM).[10,11] However, the compatibility of nanoD and nano-cBN bilayers has not been elucidated. Heteroepitaxial growth of a film on a substrate with different chemical properties is governed by two fundamental factors: (i) the lattice parameter and (ii) the surface energy. The lattice parameters of diamond and cBN differ by just 1.3%. This very small mismatch in the lattice parameters may allow heteroepitaxial growth of cBN on diamond films. However, the second condition for heteroepitaxial growth, that of favorable surface energies, must also be satisfied. If the surface energy of the material covering the surface in a thin film growth process increases the overall energy of the system, then the film being grown tends to minimize the contact area between the substrate and film. This inhibits the growth of a single-crystal layer. Therefore, the surface free energy of the film being grown should be smaller than or equal to the surface energy of the substrate to provide the opportunity for heteroepitaxial growth. Single crystalline cBN films cannot be grown heteroepitaxially on nanoD surfaces because nanoD is an inherently nanocrystalline material. However, nanocrystalline cBN might grow on nanoD in local heteroepitaxial relationships without the presence of transition noncubic BN phases given favorable relative surface energies.

The calculated surface free energies of cBN and nanoD films are approximately 40 and 55 mJ/m^2, respectively. The surface energies determined for cBN surfaces are fairly consistent with those of Keunecke et al.,[23] who reported the surface energy of their cBN films to be approximately 40 and 41 mJ/m^2 for diamond-like carbon (DLC). They also expected the surface free energy for diamond to be larger than that for DLC. This might be coincidental because neither the presented data herein nor the data in ref 23 are absolute. In addition, the cBN films discussed here and in ref 23 are different. The cBN films reported in ref 23 were prepared by sputtering a boron carbide target, which might lead to incorporation of some carbon into the cBN structure. Therefore, the determination of surface free energies for particular substrate and film structures is meaningful. The calculated surface free energies of all of the cBN films investigated herein are smaller than those of the nanoD films, which supports the viability of growing cBN films on nanoD in the absence of noncubic BN interfacial phases. Further, a local heteroepitaxial relationship can be presumed. These characteristics may also provide the outstanding adhesion properties that have already been noted. It would be worthwhile to explore further the relative surface free energies of single diamond crystals and single cBN crystals to probe the possibility of heteroepitaxial growth.

Conclusion

Cubic BN films were grown on nanoD films by plasma-enhanced CVD and PVD radio-frequency sputtering. The surface free energies of these materials were determined to evaluate the suitability of growing cBN on nanoD surfaces. All of the prepared cBN films were stoichiometric, which gave rise to the cBN phase. The rms of the smooth surface exhibited by the 500 nm cBN (rms $= 6 \pm 1$ nm), grown by sputtering at an external bias of -35 V, almost matches the surface roughness of 3 μm thick nanodiamond (rms $= 5 \pm 1$ nm). The lower effective bias used in cBN growth by ECR yielded a rougher surface morphology of 10 ± 2 nm for 500 nm cBN grown at the -20 V external bias. The least smooth surface was the 2.5 μm thick film (rms $= 37 \pm 2.5$ nm), indicating that there is an increase in surface roughness with an increase in film thickness.

The surface free energies of the films were measured employing contact angle measurements of four different liquids (water, diiodomethane, ethylene glycol, and glycerin). The liquids covered a wide range of properties from a very polar water to a very dispersive diiodomethane. The measured surface free energies of cBN and nanoD films correlate with the surface roughness. The highest surface free energy was measured for the smooth nanoD ($\sim$55 mJ/m^2) film. The surface free energies of all of the cBN films prepared exhibit lower values than those determined for the nanoD films. The relative values of the surface energies suggest that cBN can be grown without the transition noncubic BN layers and in a local heteroepitaxial relationship, which may provide outstanding cBN adhesion properties to the substrate.

Acknowledgment. This work was supported by Surface Science Western (Canada), Hong Kong RGC Grant CityU 122805, and INRS Energie, Matériaux et Télécommunications (Canada).

References and Notes

(1) Vel, L.; Demazeau, G.; Etourneau, J. *Mater. Sci. Eng., B* **1991**, *10*, 149.
(2) Bello, I.; Chan, C. Y.; Zhang, W. J.; Chong, Y. M.; Leung, K. M.; Lee, S. T.; Lifshitz, Y. *Diamond Relat. Mater.* **2005**, *143*−*7*, 1154.
(3) Ulrich, S.; Schwan, J.; Donner, W.; Ehrhardt, H. *Diamond Relat. Mater.* **1996**, *5*, 548.
(4) Miyata, N.; Moriki, K.; Mishima, O.; Fujisawa, M.; Hattori, T. *Phys. Rev. B* **1989**, *40*, 12028.
(5) Bello, I.; Chong, Y. M.; Leung, K. M.; Chan, C. Y.; Ma, K. L.; Zhang, W. J.; Lee, S. T.; Layyous, A. *Diamond Relat. Mater.* **2005**, *14*, 1784.
(6) Matsumoto, S.; Zhang, W. J. *Jpn. J. Appl. Phys.* **2000**, *39*, L442.
(7) Kester, D. J.; Ailey, K. S.; Davis, R. F. *Diamond Relat. Mater.* **1994**, *3*, 332.
(8) Medlin, D. L.; Friedmann, T. A.; Mirkarimi, P. B.; Rez, P.; McCarty, K. F.; Mills, M. J. *J. Appl. Phys.* **1994**, *76*, 295.
(9) McKenzie, D. R.; McFall, W. D.; Reisch, S.; James, B. W.; Falconer, I. S.; Boswell, R. W.; Persing, H.; Perry, A. J.; Durander, A. *Surf. Coat. Technol.* **1996**, *78*, 255.
(10) Zhang, W. J.; Bello, I.; Lifshitz, Y.; Chan, K. M.; Meng, X. M.; Wu, Y.; Chan, C. Y.; Lee, S. T. *Adv. Mater.* **2004**, *16*, 1405.
(11) Zhang, X. W.; Boyen, H. G.; Deyneka, N.; Ziemann, P.; Banhart, F.; Schreck, M. *Nat. Mater.* **2003**, *2*, 312.
(12) Zhang, W. J.; Chan, C. Y.; Chan, K. M.; Bello, I.; Lifshitz, Y.; Lee, S. T. *Appl. Phys. A* **2003**, *76*, 953.
(13) Zhang, W. J.; Matsumoto, S. *J. Mater. Res.* **2000**, *15*, 2677.
(14) Matsumoto, S.; Zhang, W. J. *Diamond Relat. Mater.* **2001**, *10*, 1868.
(15) Matsumoto, S.; Zhang, W. J. *New Diamond Front. Carbon Technol.* **2001**, *11*, 1.
(16) Mirkarimi, P. B.; McCarty, K. F.; Medlin, D. L. *Mater. Sci. Eng., R* **1997**, *21*, 47.

(17) Geick, R.; Perry, C. H.; Rupprecht, G. *Phys. Rev.* **1966**, *146*, 543.
(18) Leung, K. M.; Li, H. Q.; Zou, Y. S.; Ma, K. L.; Chong, Y. M.; Ye, Q.; Zhang, W. J.; Lee, S. T.; Bello, I. *Appl. Phys. Lett.* **2006**, *88*, 241922.
(19) Brafman, O.; Lengyel, G.; Mitra, S. S.; Gielisse, P. J.; Plendl, J. N.; Mansur, L. C. *Solid State Commun.* **1968**, *6*, 523.
(20) Young, T. *Philos. Trans. R. Soc. London* **1805**, *9*, 255.
(21) Fowkes, F. M. *Adv. Chem.* **1964**, *43*, 1.
(22) Owens, D. K.; Wendt, R. C. *J. Appl. Polym. Sci.* **1969**, *13*, 1741.
(23) Keunecke, M.; Yamamoto, K.; Bewilogua, K. *Thin Solid Films* **2001**, *398*, 142.